Carbon 127 (2018) 527–532

Contents lists available at ScienceDirect

Carbon

journal homepage: www.elsevier.com/locate/carbon

# Monoclinic $C_{16}$: $sp^2$-$sp^3$ hybridized nodal-line semimetal protected by *PT*-symmetry

Xing Feng [a], Quansheng Wu [b], Yong Cheng [a], Bin Wen [a, *], Qian Wang [c, **], Yoshiyuki Kawazoe [d], Puru Jena [e]

[a] State Key Laboratory of Metastable Materials Science and Technology, Yanshan University, Qinhuangdao, 066004, China
[b] Theoretical Physics and Station Q Zurich, ETH Zurich, 8093, Zurich, Switzerland
[c] Center for Applied Physics and Technology, College of Engineering, Peking University, Beijing, 100871, China
[d] New Industry Creation Hatchery Center, Tohoku University, 6-6-4 Aramaki-aza-Aoba, Aoba-ku, Sendai, 980-8579, Japan
[e] Department of Physics, Virginia Commonwealth University, Richmond, VA, 23284, USA

ARTICLE INFO

*Article history:*
Received 25 August 2017
Received in revised form
22 October 2017
Accepted 18 November 2017
Available online 20 November 2017

ABSTRACT

Based on first-principles calculations and Wannier tight-binding model, a three-dimensional (3D) carbon structure, named mC16, composed of interpenetrating graphene, is shown to be a topological nodal-line semimetal. The band structure calculations reveal that mC16 exhibits some exceptional properties. These include the Dirac band and band inversion around the Fermi level, and four nodal-lines in the entire Brillouin zone, symmetrically distributed on both sides of the mirror plane, and protected by the ***PT*** symmetry. In addition, the topological "drumhead-like" surface states appear on the (001) surface of mC16 and the double "drumhead-like" flat surface state emerges on the type-II (001) surface of the 3D mC16 structure. Moreover, the exotic surface Dirac points are located on the type-I (001) surface, implying that mC16 may process interesting surface transport properties. These new features make mC16 a new member in the topological carbon family, with promising novel applications in electronic device.



## 1. Introduction

Recent discoveries of topological semimetals have attracted considerable attention, due to their fascinating physical properties and potential applications [1–13]. In the large family of topological semimetals, topological carbon materials are particularly interesting because of their structural diversity and novel properties. Especially, the discovery of Dirac cone [14,15], massless Dirac fermions [14,15], and the unconventional quantum Hall effect [9,14] in graphene, significantly contributed to the interest on topological semimetals. Nevertheless, the Dirac cone in two-dimensional (2D) carbon is fragile and can be hardly applied in 3D practical device [16]. Consequently, 3D carbon topological semimetals (3D-CTSMs) are of current interest. Because of the topological properties of graphene, it is natural to use graphene as the basic building blocks for 3D-CTSMs. Accordingly, many topological carbon structures, such as triangular graphene network (TGN) [17], quadrilateral graphene network (QGN) [17], hexagonal graphene network (HGN) [17], carbon-Kagome-lattice family (CLK) structures [18], and Mackay-Terrones crystal (MTC) [16], have been predicted in the last decade. Very recently, a series of stable interpenetrating graphene networks (IGNs) have been predicted [19–23] and experimentally synthesized [23,24]. It was reported that some of IGNs possess the topological nodal-line states. A better understanding of the origin of topological nodal-line in carbon materials is not only a foundational scientific issue, but also important for designing and synthesizing 3D carbon networks with novel topological nodal-line states. Here, we propose a typical structure of IGNs, namely monoclinic C16 (mC16) structure with the topological nodal-line state, protected by coexistence of time reversal symmetry (***T***) and spatial symmetry (***P***) rather than mirror reflection symmetry.

## 2. Calculation method

Our calculations are performed within the density functional

* Corresponding author.
** Corresponding author.
*E-mail addresses:* wenbin@ysu.edu.cn (B. Wen), qianwang2@pku.edu.cn (Q. Wang).

https://doi.org/10.1016/j.carbon.2017.11.046
0008-6223/

theory (DFT) [25,26] with the projector-augmented wave (PAW) [27] method, implemented in Vienna ab initio simulation package (VASP) [28–30]. The generalized gradient approximation (GGA) in the form of Perdew-Burke-Ernzerhof (PBE) [31] is used for the exchange-correlation potential. The plane-wave cutoff energy is 500 eV, and the *k*-point separation in Brillouin Zone of the reciprocal space is taken to be $2\pi \times 0.02$ Å$^{-1}$ using the Monkhorst-Pack method. Forces on the ions are calculated according to the Hellmann-Feynman theorem, and the convergence thresholds for total energy and ionic force component are set to $1 \times 10^{-6}$ eV and 0.001 eV/Å, respectively. The phonon frequencies are obtained using the finite displacement method implemented in the PHONOPY code [32]. First-principles molecular dynamics (MD) simulations, with time steps of 1 fs (*fs*) in a supercell of $3 \times 1 \times 5$ that contain 240 carbon atoms, are also performed using the canonical (NVT) ensemble to examine the structural stability. The nodal-line search and surface states calculations are done using the open-source software Wannier_tools [33] which is based on Wannier tight-binding model constructed by Wannier90 code [34].

## 3. Results and discussion

Taking graphene sheet as the basic building block, a mixed $sp^2$-$sp^3$ hybridized 3D carbon network is constructed as shown in Fig. 1a. The optimized structure has a monoclinic primitive cell containing 16 carbon atoms with a space group ***C2/m*** (No. 12). Therefore, we name it as mC16. Its optimized lattice parameters are a = 12.7988 Å, b = 2.4461 Å, c = 4.2766 Å, and β = 88.41°. In this structure, there are four nonequivalent carbon atoms, occupying (0.75385, 0, 0.92131), (0.22631, 0, 0.42619), (0.89021, 0, 0.53077) and (0.44394, 0, 0.51593) sites, respectively. The special atomic configuration endows mC16 with a low density of 2.31 g/cm$^3$ and bulk modulus of 277 GPa, showing a high surface-to-volume ratio, and remarkable porosity, which may lead to many potential applications in batteries and catalysis [13].

Although mC16 exhibits porous character, it is a highly stable carbon allotrope. From the phonon spectra shown in Fig. 1d, one can see that no imaginary frequencies appear throughout the entire Brillouin zone (BZ), confirming that mC16 is dynamically stable at ambient pressure. Moreover, the average binding energy per atom of mC16 is only 0.161 eV and 0.063 eV higher than that of graphite and diamond, respectively, while lower than that of the theoretically predicted 3D carbon allotropes including M-carbon, and bct-$C_{12}$, and the experimentally identified fullerene $C_{60}$ as well, see Fig. 1c. This implies that mC16 could be synthesized.

In addition, the calculated independent elastic constants for mC16 are as follows:

$C_{11}$ = 656.5 GPa, $C_{12}$ = 90.8 GPa, $C_{13}$ = 54.8 GPa, $C_{16}$ = 37.7 GPa, $C_{22}$ = 1037.2 GPa, $C_{23}$ = 47.6 GPa, $C_{26}$ = 12.4 GPa, $C_{33}$ = 404.3 GPa, $C_{36}$ = 6.6 GPa, $C_{44}$ = 293.1 GPa, $C_{45}$ = 21.2 GPa, $C_{55}$ = 189.6 GPa, $C_{66}$ = 25.2 GPa.

They meet the Born criteria well [35] for monoclinic crystal, further confirming the mechanical stability of mC16. First-principles molecular dynamics simulations at 300 K with a supercell of $3 \times 1 \times 5$ containing 240 carbon atoms are also carried out. There is little change in the structure of mC16, after heating for more than 5 ps. This suggests that mC16 is thermally stable at room temperature as well.

Having confirmed the stability of mC16, we next study its electronic properties. Fig. 2a clearly shows the Dirac feature of linear dispersion of the valence and conduction bands near the Fermi level. From Fig. 2b, one can note that the density of states of mC16 is almost zero at the Fermi level, which suggests that mC16 is semimetallic. There are two band crossing points which are located

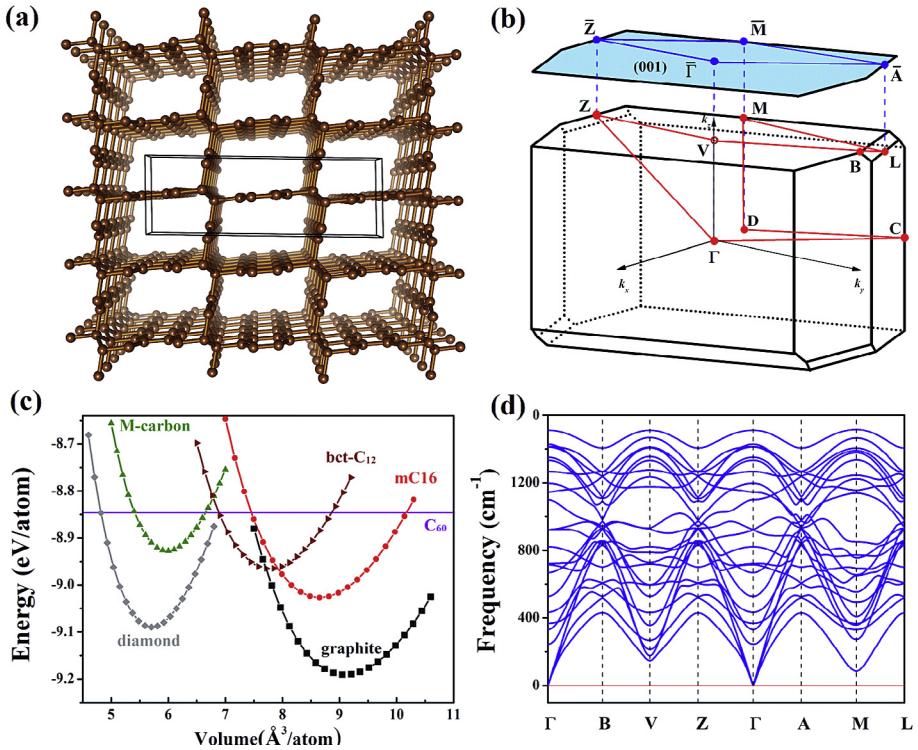


**Fig. 1. Crystal structure and its stability.** (a) Perspective view of the crystalline structure of mC16. The black cube represents the unit cell of mC16. (b) Bulk BZ and the projected BZ of the (001) surface. (c) Total energy per atom as a function of volume for graphite, diamond, mC16, bct-$C_{12}$, M-carbon and $C_{60}$ fullerene molecule. The corresponding total energies of these allotropes are −9.188, −9.090, −9.027, −8.965, −8.928, and −8.847 eV/atom, respectively. (d) Phonon spectra of mC16 at zero pressure. (A colour version of this figure can be viewed online.)

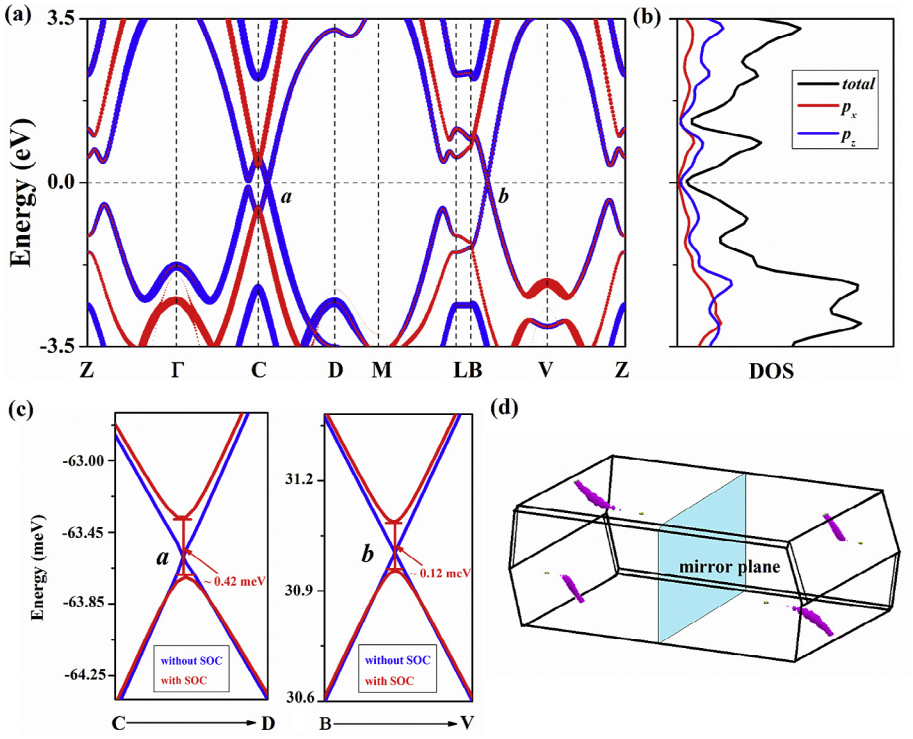


**Fig. 2. Electronic properties of mC16.** (a) Calculated energy band structures of the $p_x$ and $p_z$ orbitals along the high-symmetry points. The ***a*** and ***b*** points represent the crossing points. (b) Partial DOS of mC16. The Fermi level is set to zero. (c) Comparison of energy bands without and with SOC to the ***a*** and ***b*** points. SOC opens gaps of 0.42 meV and 0.12 meV for ***a*** and ***b*** points, respectively. (d) Fermi surface of mC16. The color plane represents the mirror plane of the BZ. (A colour version of this figure can be viewed online.)

along the C-D and B-V lines (marked as ***a*** and ***b*** point in Fig. 2a), respectively. These band crossing points deviates from the Fermi level about −63 meV and 30 meV (as shown in Fig. 2c), respectively. To investigate the formation mechanism of these crossing points further, orbital-character analysis is performed. As shown in Fig. 2a and b, $p_x$ and $p_z$ orbitals are dominant at the ***a*** and ***b*** points. Moreover, there is also a clear signature of band inversion at the ***a*** and ***b*** points, implying possible nontrivial band topological features of mC16. Since the lowest conduction band and the highest valence band along this line have opposite parities with respect to the C2 operation in the group of C-D and B-V, they can touch each other without opening a gap, thus, forming a topological semimetal. Interestingly, there are some energy bands with small slope along L-B line, which connect with the Dirac bands along B-V line as shown in Fig. 2a. It is known that Dirac band and flat band represent two extreme ends of energy bands, which can coexist in Kagome lattice [18,36–38]. This interesting phenomenon implies that mC16 may exhibit superconducting property. In addition, the spin-orbit coupling (SOC) effect opens gaps about 0.42 meV and 0.12 meV at the crossing points along the C-D and B-V lines, as shown in Fig. 2c. Such gaps indicate that the effect of SOC on the electronic band structure of mC16 is quite weak and can be ignored.

To study the electronic structure near Fermi level, the Fermi surface of mC16 is calculated as shown in Fig. 2d. The Fermi surface has four banana-like features, symmetrically distributed on both sides of the mirror plane. These four Fermi surfaces separate from each other and deviate from a certain plane. Such banana-like Fermi surface is evidence of a topological nodal-line system.

To further clarify the details of the nodal-line in mC16, a tight-binding model (WTB) based on maximally localized Wannier function is constructed, and the nodes' distribution in 3D BZ is calculated. The results are shown in Fig. 3c, which shows four nodal-lines in the entire BZ, consistent with the Fermi surface calculations. In particular, the Berry phase (a $Z_2$-type invariant) of the ***b*** point (as shown in Fig. 3c) equals $\pi$ for the k-path chosen in plane. This nonzero quantized Berry phase further confirms the nodal-line feature in mC16.

In previous studies, nodal-lines in carbon materials, such as in Mackay-Terrones crystal (MTC) [16], sc-C96 [39], and bct-C16 [40], lie almost in a certain mirror reflection plane. Once the mirror plane is destroyed, the nodal-lines would be affected in these materials. However, nodal-lines in mC16 are not in a mirror plane and are symmetrically distributed at two sides of the mirror plane. This is remarkably different with previously reported nodal-lines in carbon materials. To verify mC16 is a ***PT*** symmetry protected crystal, symmetry analysis is performed for mC16. When SOC is absent, the system can be considered as a spin-less system for which ***T*** is simply a complex conjugate operator. Therefore, we only need to consider the influence of ***P*** symmetry on the Bloch functions. For the primitive cell of mC16, its inversion center can be defined as,

$$I : (x, y, z) \rightarrow (-x, -y, -z).$$

And the mirror reflection symmetry can be defined as,

$$M : (x, y, z) \rightarrow (y, x, z).$$

In momentum space,

$$M : (k_x, k_y, k_z) \rightarrow (k_y, k_x, k_z).$$

Thus, mC16 is a centrosymmetric crystal with inversion symmetry. One can adopt a gauge for the Bloch functions such that $u^*_{nk}(r) = u_{n-k}(r)$. On the other hand, inversion symmetry connects $u_{nk}(-r)$ to $u_{n-k}(r)$, and we are allowed to let $u_{nk}(-r) = u_{n-k}(r)$. Combining the above two equations, one obtains $u^*_{nk}(r) = u_{nk}(-r)$. Then, it is straightforward to show that the corresponding effective Hamiltonian $H(k)$ has to be real valued, i.e. $H_{mn}(k) = H_{nm}(k)$. A band

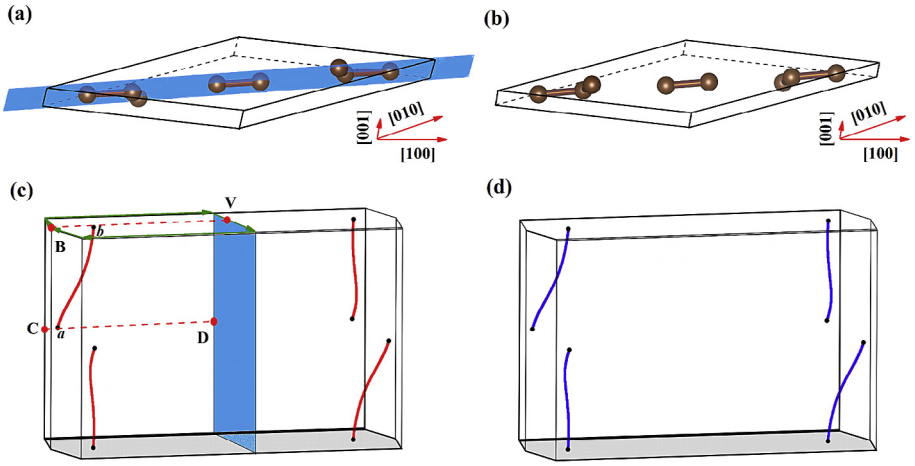


**Fig. 3. Nodal-line structure in mC16.** (a) Primitive cell of mC16. Color plane is the mirror plane of the primitive cell. The Space group is *C*2/m (No. 12), and its optimized lattice parameters are a = b = 6.5152 Å, c = 4.2766 Å, α = β = 91.5631°, and γ = 21.6395°. (b) The deformed cell of mC16. The Space group is P-1 (No. 2), and its optimized lattice parameters are a = 6.52232 Å, b = 6.5403 Å, c = 4.33438 Å, α = 92.02438°, β = 92.02416°, and γ = 21.97672°. (c) Nodal-lines structure of mC16. The green line is the path to calculate the Berry phase. The ***a* and *b*** points represent the crossing point located along C-D and B-V line, respectively. Color plane is the mirror plane of the bulk BZ. (d) Nodal-lines structure of deformed mC16. (A colour version of this figure can be viewed online.)

crossing point at an arbitrary k point can be minimally described by a two-band effective Hamiltonian, which can be expressed in terms of the identity matrix and the three Pauli matrices. According to the above argument, the two-band Hamiltonian for a system, obeying both ***T*** and ***P*** symmetries, can be chosen as real valued, so the codimension of such a band crossing point is 2, one less than the number of independent variables (i.e., $k_x$, $k_y$, and $k_z$). Hence, the nodal line in mC16 is stable in the presence of existing ***PT*** symmetries, which are enough to protect the nodal-lines in mC16. Any perturbations that preserve the inversion symmetry, can only distort the nodal-line, but not destroy them. As an example, we apply a uniaxial strain (compression 1%) along the [001] crystal direction. After deformation, the structure of mC16 belongs to space group of ***P-1*** (No. 2), which preserves the inversion symmetry, but just destroys the mirror plane in mC16. As a result shown in Fig. 3d, it is found that when the mirror plane is destroyed, the nodal-lines in mC16 still exist, rather than vanishing as the nodal-line structure is protected by mirror reflection symmetry. Thus, the nodal-lines in mC16 are robust.

One of the most important signatures of a topological nodal-line semimetal is the existence of "drumhead-like" surface states [41]. Fig. 4 shows the calculated local density of states (LDOS) for the semi-infinite (001) surface using the constructed WTB model. We choose two types of (001) surface of mC16 to calculate the surface states and surface band structure, as shown in Fig. 4a. For the type-I (001) surface, as shown in Fig. 4a, the "drumhead-like" surface states are nestled outside the projected nodal loop. The results are shown in Fig. 4b. Note that the nearly flat "drumhead-like" surface state is similar to some previous works [42] and can be considered as the hallmark of a bulk topological nodal-loop semimetal. However, the surface states for the type-II (001) surface are dramatically different. As shown in Fig. 4c, there are two surface bands emerging on the type-II (001) surface, one surface band outside the projected nodal loop just like the surface states of type-I (001) surface. The other one surface band penetrates the entire region and deviates from the projected nodal loop. These double "drumhead-like" surface states are firstly found in carbon materials, implying novel surface transport properties on the (001) surface of mC16. To our knowledge, surface states obtained from the WTB model usually are used to explain the topological properties of materials. To compare the surface states with ARPES experimental data for further use, a DFT calculation with a 20-atomatic-layer thickness slab system was performed, as shown in Fig. 4c. The DFT calculated surface states with two types of (001) surfaces show some differences with WTB results. Firstly, type-I surface states are mainly convex for WTB results; however, they are concave for DFT results. The energy of type-II surface states in WTB is higher than DFT results by about 1 eV. Secondly, as shown in Fig. 4c, there are two surface Dirac points emerging on the type-I surface, which is similar to the $TiB_2$ surface state and firstly discovered in carbon materials [43]. It means that not only the bulk states of mC16 are topological nodal-line state, but also the surface states of mC16 have Dirac points similar with graphene, which indicates some novel surface transport properties in mC16.

Recently, high-quality 3D nanoporous graphene-based structures have been fabricated successfully [44,45] and covalently bonded 3D graphene macroscopic structures have also been synthesized using chemically derived graphene sheets [46,47]. Moreover, experimental research suggests that interpenetrated graphene networks structures might locally exist within compressed glassy carbons [23,24]. These advances make the synthesis of mC16 and its expanded carbon allotropes very promising. Once synthesized, mC16 not only can be used as an ideal platform to study the topological properties, but also may find an array of potential applications as shape-selective catalyst, molecular sieves or absorbents, superconductors, and battery materials.

## 4. Conclusions

In summary, based on first-principles calculations, a new carbon allotrope, mC16, has been identified, and its topological properties have been systematically studied. The calculated results show that mC16 is a stable topological nodal-line semimetal with many novel properties. (1) There are Dirac band and band inversion around the Fermi level, and four nodal-lines in the entire Brillouin zone, symmetrically distributed on both sides of the mirror plane. (2) The topological states in mC16 are protected by PT symmetry rather than mirror reflection symmetry. (3) The "drumhead-like" surface states exist on the (001) surface, while the exotic double "drumhead-like" surface states emerge on the type-II (001) surface. These multiple-features are found for the first time in carbon materials. (4) Two surface Dirac points emerge on the type-I (001) surface of

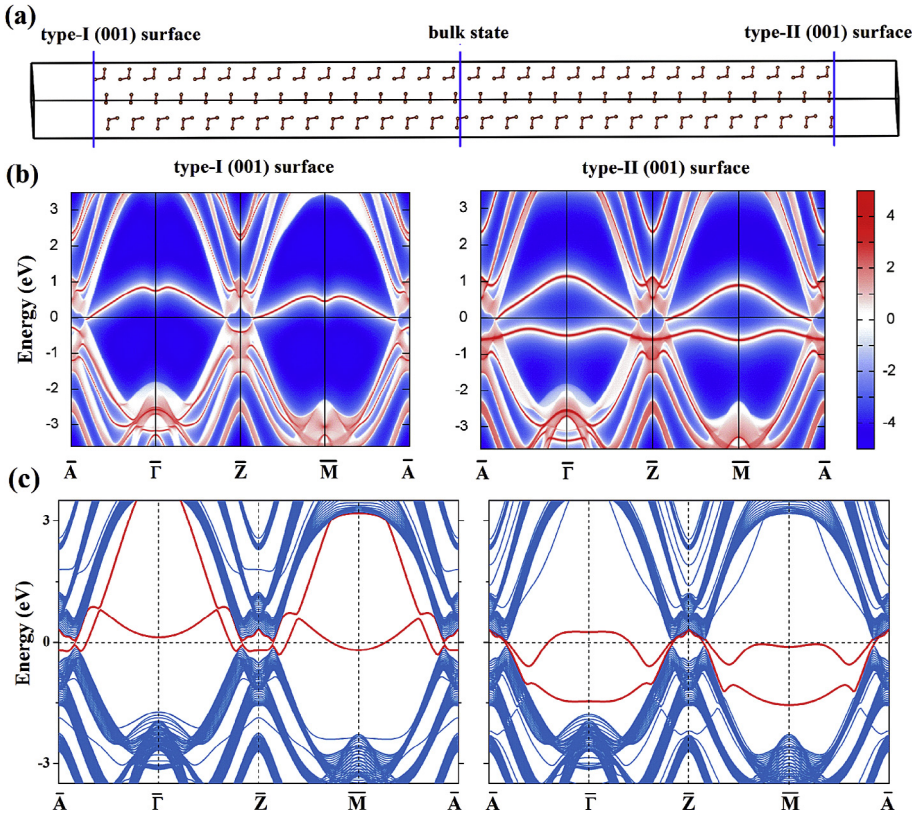


**Fig. 4. Surface states of mC16**. (a) Atomic structure of mC16 for two types of (001) surface. (b) Type-I and type-II surface states of the (001) surface obtained by WTB model. (c) Type-I and type-II surface states of (001) surface obtained from DFT calculations. (A colour version of this figure can be viewed online.)

mC16, which may lead to some special transport properties on this surface. These results not only suggest the existence of nontrivial topology in mC16 and its variants, but also provide an ideal system to explore the novel physics in carbon materials.

## Acknowledgement

This work was supported by the National Natural Science Foundation of China (NSFC-51372215, NSFC-51471004, and NSFC-51771165), and the National Key Research and Development Program of China (2016YFE0127300 and 2017YFA0205003). P.J. acknowledges support of the U. S. Department of Energy, Office of Basic Energy Sciences, Division of Materials Sciences and Engineering under Award # DE-FG02-96ER45579. The authors would like to thank the staff of the Center for Computational Materials Science, Institute for Materials Research, Tohoku University for computer support.

## References

[1] Z. Liu, B. Zhou, Y. Zhang, Z. Wang, H. Weng, D. Prabhakaran, et al., Discovery of a three-dimensional topological Dirac semimetal, $Na_3Bi$, Science 343 (6173) (2014) 864–867.
[2] Z. Liu, J. Jiang, B. Zhou, Z. Wang, Y. Zhang, H. Weng, et al., A stable three-dimensional topological Dirac semimetal $Cd_3As_2$, Nat. Mater. 13 (7) (2014) 677–681.
[3] Y. Kim, B.J. Wieder, C. Kane, A.M. Rappe, Dirac line nodes in inversion-symmetric crystals, Phys. Rev. Lett. 115 (3) (2015), 036806.
[4] R. Yu, H. Weng, Z. Fang, X. Dai, X. Hu, Topological node-line semimetal and dirac semimetal state in antiperovskite $Cu_3PdN$, Phys. Rev. Lett. 115 (3) (2015), 036807.
[5] S.-Y. Xu, I. Belopolski, N. Alidoust, M. Neupane, G. Bian, C. Zhang, et al., Discovery of a Weyl fermion semimetal and topological Fermi arcs, Science 349 (6248) (2015) 613–617.
[6] B. Lv, H. Weng, B. Fu, X. Wang, H. Miao, J. Ma, et al., Experimental discovery of weyl semimetal TaAs, Phys. Rev. X 5 (3) (2015), 031013.
[7] J. Liu, D. Kriegner, L. Horak, D. Puggioni, C. Rayan Serrao, R. Chen, et al., Strain-induced nonsymmorphic symmetry breaking and removal of Dirac semimetallic nodal line in an orthoperovskite iridate, Phys. Rev. B 93 (8) (2016).
[8] F.D.M. Haldane, Model for a quantum Hall effect without Landau levels: condensed-matter realization of the" parity anomaly", Phys. Rev. Lett. 61 (18) (1988) 2015.
[9] C.L. Kane, E.J. Mele, Quantum spin Hall effect in graphene, Phys. Rev. Lett. 95 (22) (2005), 226801.
[10] H. Zhang, C.-X. Liu, X.-L. Qi, X. Dai, Z. Fang, S.-C. Zhang, Topological insulators in $Bi_2Se_3$, $Bi_2Te_3$ and $Sb_2Te_3$ with a single Dirac cone on the surface, Nat. Phys. 5 (6) (2009) 438–442.
[11] Z. Wang, Y. Sun, X.-Q. Chen, C. Franchini, G. Xu, H. Weng, et al., Dirac semimetal and topological phase transitions in $A_3Bi$ (A= Na, K, Rb), Phys. Rev. B 85 (19) (2012), 195320.
[12] H. Weng, C. Fang, Z. Fang, B.A. Bernevig, X. Dai, Weyl semimetal phase in noncentrosymmetric transition-metal monophosphides, Phys. Rev. X 5 (1) (2015), 011029.
[13] J. Liu, S. Wang, Q. Sun, All-carbon-based porous topological semimetal for Li-ion battery anode material, Proc. Natl. Acad. Sci. (2017), 201618051.
[14] Y. Zhang, Y.-W. Tan, H.L. Stormer, P. Kim, Experimental observation of the quantum Hall effect and Berry's phase in graphene, Nature 438 (7065) (2005) 201–204.
[15] K.S. Novoselov, A.K. Geim, S.V. Morozov, D. Jiang, M.I. Katsnelson, I.V. Grigorieva, et al., Two-dimensional gas of massless Dirac fermions in graphene, Nature 438 (7065) (2005) 197–200.
[16] H. Weng, Y. Liang, Q. Xu, R. Yu, Z. Fang, X. Dai, et al., Topological node-line semimetal in three-dimensional graphene networks, Phys. Rev. B 92 (4) (2015).
[17] C. Zhong, Y. Chen, Y. Xie, S.A. Yang, M.L. Cohen, S. Zhang, Towards three-dimensional Weyl-surface semimetals in graphene networks, Nanoscale 8 (13) (2016) 7232–7239.
[18] C. Zhong, Y. Xie, Y. Chen, S. Zhang, Coexistence of flat bands and Dirac bands in a carbon-Kagome-lattice family, Carbon 99 (2016) 65–70.
[19] Z. Zhao, Theoretical and Experimental Research on Novel Structures and Properties of Carbon Group Elements and Transition Metal Carbides, PhD thesis, 2012.
[20] X. Jiang, J. Zhao, Y.L. Li, R. Ahuja, Tunable assembly of $sp^3$ cross-linked 3D graphene monoliths: a first-principles prediction, Adv. Funct. Mater. 23 (47) (2013) 5846–5853.
[21] X. Dong, M. Hu, J. He, Y. Tian, H.-T. Wang, A new phase from compression of

carbon nanotubes with anisotropic Dirac fermions, Sci. Rep. 5 (2015).
[22] Y. Chen, Y. Xie, S.A. Yang, H. Pan, F. Zhang, M.L. Cohen, et al., Nanostructured carbon allotropes with Weyl-like loops and points, Nano Lett. 15 (10) (2015) 6974–6978.
[23] Y. Lin, Z. Zhao, T.A. Strobel, R.E. Cohen, Interpenetrating graphene networks: three-dimensional node-line semimetals with massive negative linear compressibilities, Phys. Rev. B 94 (24) (2016), 245442.
[24] M. Hu, J. He, Z. Zhao, T.A. Strobel, W. Hu, D. Yu, et al., Compressed glassy carbon: an ultrastrong and elastic interpenetrating graphene network, Sci. Adv. 3 (6) (2017), e1603213.
[25] P. Hohenberg, W. Kohn, Inhomogeneous electron gas, Phys. Rev. 136 (3B) (1964) B864.
[26] W. Kohn, L.J. Sham, Self-consistent equations including exchange and correlation effects, Phys. Rev. 140 (4A) (1965) A1133.
[27] P.E. Blöchl, Projector augmented-wave method, Phys. Rev. B 50 (24) (1994) 17953.
[28] G. Kresse, J. Furthmüller, Efficiency of ab-initio total energy calculations for metals and semiconductors using a plane-wave basis set, Comput. Mater. Sci. 6 (1) (1996) 15–50.
[29] G. Kresse, J. Furthmüller, Efficient iterative schemes for ab initio total-energy calculations using a plane-wave basis set, Phys. Rev. B 54 (16) (1996) 11169.
[30] G. Kresse, D. Joubert, From ultrasoft pseudopotentials to the projector augmented-wave method, Phys. Rev. B 59 (3) (1999) 1758.
[31] J.P. Perdew, K. Burke, M. Ernzerhof, Generalized gradient approximation made simple, Phys. Rev. Lett. 77 (18) (1996) 3865.
[32] A. Togo, F. Oba, I. Tanaka, First-principles calculations of the ferroelastic transition between rutile-type and $CaCl_2$-type $SiO_2$ at high pressures, Phys. Rev. B 78 (13) (2008), 134106.
[33] Q. Wu, S. Zhang, H.-F. Song, M. Troyer, A.A. Soluyanov, WannierTools: an Open-source Software Package for Novel Topological Materials, arXiv preprint arXiv:170307789, 2017.
[34] A.A. Mostofi, J.R. Yates, Y.-S. Lee, I. Souza, D. Vanderbilt, N. Marzari, wannier90: a tool for obtaining maximally-localised Wannier functions, Comput. Phys. Commun. 178 (9) (2008) 685–699.
[35] Z-j. Wu, E-j. Zhao, H-p. Xiang, X-f. Hao, X-j. Liu, J. Meng, Crystal structures and elastic properties of superhard $IrN_2$ and $IrN_3$ from first principles, Phys. Rev. B 76 (5) (2007), 054115.
[36] E. Tang, J.W. Mei, X.G. Wen, High-temperature fractional quantum Hall states, Phys. Rev. Lett. 106 (23) (2011), 236802.
[37] Z.F. Wang, N. Su, F. Liu, Prediction of a two-dimensional organic topological insulator, Nano Lett. 13 (6) (2013) 2842.
[38] Z. Liu, Z.F. Wang, J.W. Mei, Y.S. Wu, F. Liu, Flat chern band in a two-dimensional organometallic framework, Phys. Rev. Lett. 110 (10) (2013), 106804.
[39] Y. Cheng, J. Du, R. Melnik, Y. Kawazoe, B. Wen, Novel three dimensional topological nodal line semimetallic carbon, Carbon 98 (2016) 468–473.
[40] Y. Cheng, X. Feng, X. Cao, B. Wen, Q. Wang, Y. Kawazoe, et al., Body-centered tetragonal C16: a novel topological node-line semimetallic carbon composed of tetrarings, Small 13 (12) (2017).
[41] H. Huang, J. Liu, D. Vanderbilt, W. Duan, Topological nodal-line semimetals in alkaline-earth stannides, germanides, and silicides, Phys. Rev. B 93 (20) (2016), 201114.
[42] G. Bian, T.-R. Chang, H. Zheng, S. Velury, S.-Y. Xu, T. Neupert, et al., Drumhead surface states and topological nodal-line fermions in $TlTaSe_2$, Phys. Rev. B 93 (12) (2016), 121113.
[43] X. Feng, C. Yue, Z. Song, Q. Wu, B. Wen, Topological Dirac Nodal-net Fermions in $AlB_2$-type $TiB_2$ and $ZrB_2$, arXiv preprint arXiv:170500511, 2017.
[44] Y. Ito, H.J. Qiu, T. Fujita, Y. Tanabe, K. Tanigaki, M. Chen, Bicontinuous nanoporous N-doped graphene for the oxygen reduction reaction, Adv. Mater. 26 (24) (2014) 4145–4150.
[45] Y. Ito, Y. Tanabe, H.J. Qiu, K. Sugawara, S. Heguri, N.H. Tu, et al., High-quality three-dimensional nanoporous graphene, Angew. Chem. Int. Ed. 53 (19) (2014) 4822–4826.
[46] M.A. Worsley, T.Y. Olson, J.R. Lee, T.M. Willey, M.H. Nielsen, S.K. Roberts, et al., High surface area, $sp^2$-cross-linked three-dimensional graphene monoliths, J. Phys. Chem. Lett. 2 (8) (2011) 921.
[47] Z. Chen, W. Ren, L. Gao, B. Liu, S. Pei, H.M. Cheng, Three-dimensional flexible and conductive interconnected graphene networks grown by chemical vapour deposition, Nat. Mater. 10 (6) (2011) 424–428.